KONA Powder and Particle Journal

KONA Powder and Particle Journal No. 42 (2025) 241–250/https://doi.org/10.14356/kona.2025009 Original Research Paper

Rheological Characterization of Mineral Slurries Based on the Principle of Maximum Entropy †

Jean C. G. Louzada [1], Elaine C. Andrade [2], Thiago C. Souza Pinto [3] and Laurindo S. Leal Filho [2]*

[1] *Geosciences and Engineering Institute, Federal University of Southern and Southeastern Pará, Brazil*
[2] *Department of Mining and Petroleum Engineering, Polytechnic School, University of São Paulo, Brazil*
[3] *Mineral Development Center (CDM), Vale S.A., Brazil*

The rheological characterization of mineral slurries is a complex task, especially in the presence of coarse particles with high specific gravity, such as hematite. In laboratory rotational rheometers (LRRs), entrance effects, particle settling, and Taylor vortices can jeopardize the accuracy of the results. This paper presents a new methodology for the rheological characterization of mineral slurries in tubular devices and the Principle of Maximum Entropy (PME) supports this new approach. Iron ore slurries were prepared at mass concentrations of 36.8 % and 43.6 % solids and subjected to rheological characterization in LRR and a pumping loop tubular device (PLTD). The results from LRR revealed shear-thickening behavior for the slurries; whereas the results from PLTD, associated with entropic equations for the friction factor and shear rate, revealed shear-thinning behavior (at low shear rates) and shear-thickening behavior (at high rates). The results from LRR plus PLTD were plotted in a single rheogram, and curve fitting was accomplished by the power law model ($R^2 = 0.995$), indicating an overall shear-thickening behavior. PME proved to be capable of supporting the rheological characterization of mineral slurries at shear rates above 1500 s^{-1} in PLTD, complementing the results obtained by LRR.

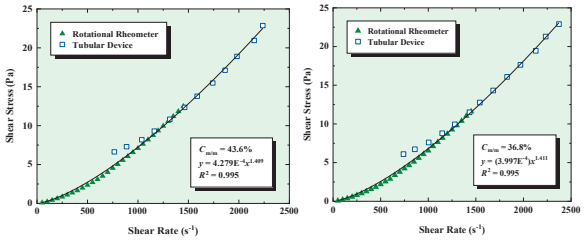

Keywords: rheometry, mineral slurries, the principle of maximum entropy

1. Introduction

Ores are often beneficiated in the form of slurries, which are subjected to different unit operations of mineral processing. Consequently, concentrates and tailings are also yielded as particulate suspensions, which are classified as pseudo-homogeneous fluids and exhibit complex rheological behavior (Kawatra and Bakshi, 1995). Thus, the rheology of mineral slurries is of vital importance for determining the operating conditions of flow (flow velocity and head loss), for the design and selection of pipelines and pumps, and for estimating energy consumption (Whiten et al., 1993).

The rheological characterization of mineral slurries presents many challenges, especially when performed in rotational rheometers and in the presence of coarse particles with high specific gravity. Under these conditions, wall slipping effects (Mooney, 1931; Senapati and Mishra, 2014), particle settling (Kawatra and Bakshi, 1996; Klein and Laskowski, 2000), centrifugal force (Mezger, 2020), and Taylor vortices (Pereira and Soares, 2012; Shi, 2016) recur. Such effects isolated or associated, can significantly jeopardize the accuracy of measurements. Therefore, an alternative to rotational and tube-capillary devices would be a tubular apparatus (test-loop experimental facility) that reproduces real flow conditions, i.e., turbulent flows, with high shear rates in rough pipes of larger diameters.

From an experimental perspective, previously existing challenges can be overcome with tubular devices of the pumping loop type. However, there is a gap in the literature regarding the determination of shear rate for turbulent flow of non-Newtonian fluids, since the established Rabinowitsch–Mooney model was developed for the laminar regime (Chilton and Stainsby, 1998; Chhabra and Richardson, 1999). Thus, the objective of this work is to present and propose a new methodology, based on the Principle of Maximum Entropy (PME), for shear rate and apparent viscosity determination of mineral slurries in pumping loop tubular devices (PLTD) because they can operate under experimental conditions that are closer to the reality of flow in pipes. The model used in this work for shear rate was obtained from the entropic velocity distribution maintained by Chiu et al. (1993) and developed for flow in tubes, which is applicable to Newtonian and

† Received 2 August 2023; Accepted 24 August 2023
J-STAGE Advance published online 13 April 2024
* Corresponding author: Laurindo S. Leal Filho;
Add: Av. Professor Melo Moraes, 2373–Cidade Universitária–CEP 05508-900, São Paulo-SP, Brazil
E-mail: lauleal@usp.br
TEL: +55-11-99981-1037

non-Newtonian fluids in laminar and turbulent regimes, regardless of tube roughness (Louzada et al., 2021).

1.2 Theoretical background

Rheology is classically defined as the science that studies the flow and deformation of matter under the action of external forces (Slatter, 2000). The rheological behavior of a fluid is described by the functional relationships between shear stress and shear rate or between viscosity and shear rate, which are governed by constitutive rheological equations (Peker and Helvaci, 2007).

Laboratory rotational rheometers (LRRs) were designed based on the dynamics of circular movements. In these devices, the torque is determined as a function of the angular velocity applied to the sensor in contact with the fluid. Stress and shear rate are calculated from the torque and angular velocity, respectively, through specific correlations for each sensor. LRR are classified according to sensor geometry into concentric cylinders, cone plates, parallel plates, vanes, and Mooney–Ewart (Barnes et al., 1989; Boger, 2009; Kelessidis and Maglione, 2008).

The most widely used rotational device is the concentric cylinder type, in which the fluid is confined in the annular space between the inner and outer cylinders. In the Searle system, the outer cylinder remains at rest, while the inner cylinder rotates. High rotational speeds can cause centrifugal force effects, secondary flows, and Taylor vortices, which can jeopardize the accuracy of the measurements (Mezger, 2020; Shi, 2016). **Eqns. (1)** and **(2)** allow the calculation of the shear rate ($\dot{\gamma}$) and shear stress (τ) referring to the Mooney–Ewart sensor used in this work (Mezger, 2020).

$$\dot{\gamma} = \omega \frac{1+\delta^2}{\delta^2 - 1} \tag{1}$$

$$\tau = \frac{1+\delta^2}{2\delta^2} \frac{T}{2\pi L R_i^2 C_L} \tag{2}$$

The flow conditions in a concentric cylinder-type device operating in the Searle system can be determined from the Taylor number *(Ta)*, defined according to **Eqn. (3)** (Shi, 2016). Therefore, according to the magnitude of the Taylor number, the following flow regimes are defined (Shi, 2016): i) laminar if $Ta < 41.3$; ii) laminar as vortices begin to appear when $41.3 < Ta < 400$; iii) Turbulent for $Ta > 400$.

$$Ta = \frac{(R_e - R_i) u_{ci} \rho}{\eta} \sqrt{\frac{R_e - R_i}{R_i}} \tag{3}$$

Tubular rheometers are devices of simple design, essentially built with circular tubes and equipped with a pumping system, flow, and pressure meters (Fangary et al., 1997; Giguère et al., 2009). The rheological characterization performed in these devices is called an inverse problem in rheology, in which the shear stress (τ_w) and shear rate ($\dot{\gamma}_w$) are determined from the pressure gradient ($\Delta P/L$) and mean velocity of fluid flow ($\bar{u}$), according to **Eqns. (4)** and **(5)**, respectively (Boger, 2009; Ma et al., 2012).

$$\tau_w = \left(-\frac{\Delta P}{L}\right).\left(\frac{D}{4}\right) \tag{4}$$

$$\dot{\gamma}_w = \frac{8\bar{u}}{D} \tag{5}$$

Eqn. (4) is used for any type of fluid regardless of the flow regime. On the other hand, **Eqn. (5)** is applied only to fluids with Newtonian behavior and laminar flow regime. For fluids with non-Newtonian behavior and laminar flows, the shear rate can be determined from the Rabinowitsch–Mooney model, as expressed by **Eqn. (6)**. In this model, the correction factor n' is determined from the shear stress, mean velocity flow, and pipe diameter, according to **Eqn. (7)** (Chhabra and Richardson, 1999; Kitanovski et al., 2005; Lu and Zhang, 2002; Metzner and Reed, 1955).

$$\dot{\gamma}_w = \left(\frac{8\bar{u}}{D}\right)\left(\frac{3n'+1}{4n'}\right) \tag{6}$$

$$n' = \frac{d(\ln \tau_w)}{d\left[\ln\left(\frac{8\bar{u}}{D}\right)\right]} \tag{7}$$

1.2.1 The principle of maximum entropy (PME)

The term entropy is not restricted to the thermodynamic state function. In the context of information theory, entropy is a measure of information or uncertainty about a given variable (Singh et al., 2017). For continuous random variables, Claude Shannon defined the entropy of a variable (u) according to **Eqn. (8)** (Chiu, 1989), where $f(u)$ is the probability density function of u.

$$H(u) = -\int_0^{u_{max}} f(u) \ln f(u) \, du \tag{8}$$

In his work, Chiu (1987) applied PME to hydraulic engineering, developing physically consistent models for velocity distributions, shear stress, and sediment concentration in open channels. The application of PME to fluid flow essentially consists of determining velocity entropy from **Eqn. (8)** and maximizing it based on Lagrange multipliers (Singh, 2014). PME and the maximization technique were applied by Chiu et al. (1993) to obtain velocity distributions for flows in tubes, defined by **Eqn. (9)** and applicable to fluids with Newtonian and non-Newtonian behaviors, regardless of the flow regime and roughness of the tube.

$$u_E(r) = \left(\frac{u_{max}}{M}\right) \ln\left\{1 + \left[e^M - 1\right]\left[1 - \left(\frac{r}{R}\right)^2\right]\right\} \tag{9}$$

Eqn. (10) correlates the entropic shear rate, $\dot{\gamma}_{w(E)}$ defined as the velocity gradient in the wall, with the entropic parameter (M), mean flow velocity ($\bar{u}$), and tube internal diameter (D) (Louzada et al., 2021).

$$\dot{\gamma}_{w(E)}=\left(-\frac{du_E}{dr}\right)\Bigg|_{r=R}=\left(\frac{8\bar{u}}{D}\right)\left[\frac{(e^M-1)^2}{2(Me^M-e^M+1)}\right] \quad (10)$$

Once obtained from a universal velocity distribution, **Eqn. (10)** allows the determination of the shear rate for any type of fluid, in the laminar or turbulent regime, and regardless of tube roughness. The literature also reports a model for the friction factor expressed as a function of the apparent Reynolds number (Re_a) and the entropy parameter (M), as shown in **Eqn. (11)** (Souza and Moraes, 2017).

$$f_E=\left(\frac{32}{Re_a}\right)\left[\frac{(e^M-1)^2}{(Me^M-e^M+1)}\right] \quad (11)$$

In a more recent contribution, Louzada et al. (2021) proposed a model for the entropic friction factor, defined only as a function of the entropy parameter, according to **Eqn. (12)**.

$$f_E=\frac{32}{[416.667(e^M-1)]^{\frac{1}{1.0028}}}\left[\frac{(e^M-1)^2}{(Me^M-e^M+1)}\right] \quad (12)$$

In the present work, **Eqn. (12)** is used to determine parameter M, using friction factor values obtained previously from the experimental data of the pressure gradient ($\Delta P/L$) and mean flow velocity ($\bar{u}$) resorting to the Darcy–Weissbach equation (**Eqn. (13)**).

$$\frac{\Delta P}{\rho g}=f\frac{L}{D}\frac{\bar{u}^2}{2g} \quad (13)$$

The apparent viscosity (η) is calculated from the well-known **Eqn. (14)**.

$$Re_a=\frac{\bar{u}D\rho}{\eta} \quad (14)$$

2. Materials and methods

2.1 Technological characterization of iron ore

The mining company Vale SA provided the iron ore sample used in this work. It comes from Carajás, Pará, Brazil. The technological characterization of the ore consisted of determining its mineralogical composition, chemical composition, particle size distribution, and specific gravity. The mineralogy was determined by X-ray diffraction (X'Pert Diffractometer, Philips 1997), in which the following minerals were identified: hematite, goethite, quartz, and magnetite. The chemical composition of the ore by X-ray fluorescence (Malvern Panalytical–Zetium Model) is shown in **Table 1**. Results on particle size distribution by laser diffraction (Mastersizer 2000–Malvern Instruments Ltd) are reported in **Table 2**. The specific gravity (4805 kg/m^3) of the iron ore was determined by gas pycnometry (Quantachrome pycnometer) using a cell with a volume of 150.87 cm^3. The measurement was performed at 21.8 °C by using nitrogen.

Table 1 Chemical analysis of the iron ore.

Elements	Grade (%)
Fe	64.3
SiO_2	2.50
Al_2O_3	1.50
P	0.077
Mn	0.22
TiO_2	0.13
CaO	<0.10
MgO	<0.10
LOI	3.44

Table 2 Size analysis of the iron ore.

$d_{3,2}$ (μm)	d_{10} (μm)	d_{50} (μm)	d_{90} (μm)
4.37	1.55	21.54	76.25

2.2 Rotational rheometry

Rotational rheometry experiments were conducted in an Anton Paar MCR 92 rheometer equipped with the RheoCompassTM software and operating on the Searle system. In this study, a Mooney–Ewart-type sensor (CC39) was used. The diameters of the inner and outer cylinders are 38.716 mm and 42.010 mm, respectively. The height of the inner cylinder corresponds to 60.014 mm, and the angle of the conical surface is 120°.

The experiments were carried out with slurries prepared at concentrations of 36.8 % and 43.6 % of solids (mass basis), and the shear rate values were kept in the range of 50 s^{-1} and 1450 s^{-1}. The specific gravities of the slurries were: 1363.2 kg/m^3 and 1483.7 kg/m^3 for solid concentrations of 36.8 % and 43.6 %, respectively. The experiments were carried out after a previous stirring step for 120 seconds, at a shear rate of 1450 s^{-1}, in order to keep the particles suspended and mitigate the sedimentation effect. Once the 120 second stirring time elapsed, the shear rate was gradually reduced from 1450 s^{-1} to the final value of 50 s^{-1}. The experimental results were submitted to curve fitting using the Power Law and Tscheuschner rheological models (Tozzi and Hartt, 2021).

2.3 Tubular rheometry

A tubular device constructed with a pipe with an internal diameter of 76.2 mm was used in the tubular rheometry tests (**Fig. 1**). Horizontal sections of the pipeline were constructed in perspex sections to allow flow visualization. The experimental apparatus consists of a tank, a pump, and a pipeline endowed with flow and pressure sensors. The tank has a usable volume of 1 m^3, and is equipped with a stirrer driven by a 6 HP WEG electric motor controlled by

a frequency inverter (WEG–CFW 500). The slurry was transported by a Warman centrifugal pump, model 4/3C-AH, driven by a 22 kW WEG W22 electric motor at a nominal speed of 1765 rpm, and controlled by a WEG frequency inverter, model CFW700. Pressure transducers (Siemens) and flow meters (Krohne Connaut) provided data regarding pressure drop and volumetric flow. The process variables were monitored and stored using a data acquisition system equipped with a digital indicator (DMY-2015 model) and VR2000 software version 3.3, both manufactured by Presys.

The experimental procedure consisted of hydraulic transport, in a closed circuit, of the slurries prepared at the same solid concentrations as in the rotational rheometry tests. The pressure differences (ΔP) corresponding to the operating volumetric flows *(Q)* were measured.

From these experimental data, the friction factor was calculated from the Darcy–Weisbach equation. Shear stress (τ_w), entropic shear rate ($\dot{\gamma}_{w(E)}$), apparent Reynolds number (Re_a), parameter M, and apparent viscosity (η), were determined using **Eqns. (4)**, **(10)**, **(11)**, **(12)**, and **(14)**, respectively.

3. Results and discussion

3.1 Rotational rheometry

The results of the shear stress as a function of shear rate, obtained by rotational rheometry, are shown in **Fig. 2**.

All suspensions behaved as shear-thickening fluids, with viscosity increasing with the increase in the shear rate, as observed in **Fig. 3**.

Furthermore, for the same shear rate, the slurry viscosity increases with increasing solids concentration. The behavior indices (n) referring to the suspensions with 36.8 % and 43.6 % solids showed values of 1.532 and 1.493, respectively, as shown in **Table 3**, corroborating the shear-thickening behavior. According to Brown and Jaeger (2014), when the behavior index (n) reveals values between 1 and 2, the fluid is classified as continuous shear thickening.

The experimental data were also adjusted using the Tscheuschner model, as shown in **Table 4**. The Bingham model was not used because it is inadequate to fit experimental data that follow nonlinear behavior at lower shear rates (Boger, 2009; Slatter, 2000).

Inertial effects and the possible occurrence of Taylor vortices were also investigated in rotational rheometry experiments. The peripheral velocity of the sensor was

Fig. 1 Test-loop experimental facility.

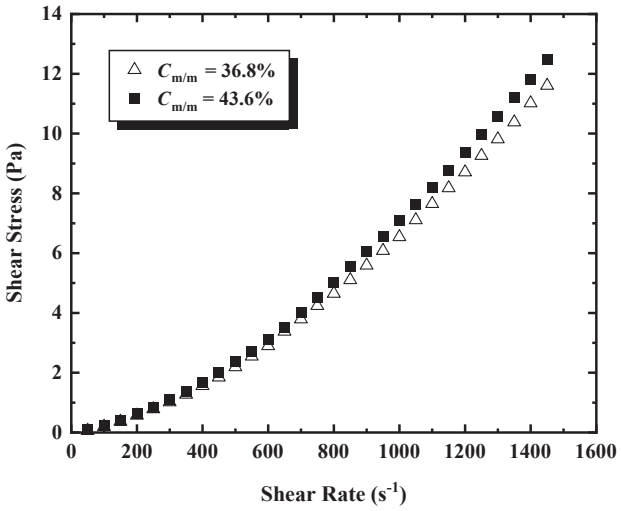

Fig. 2 Shear stress as a function of the shear rate, obtained by rotational rheometry.

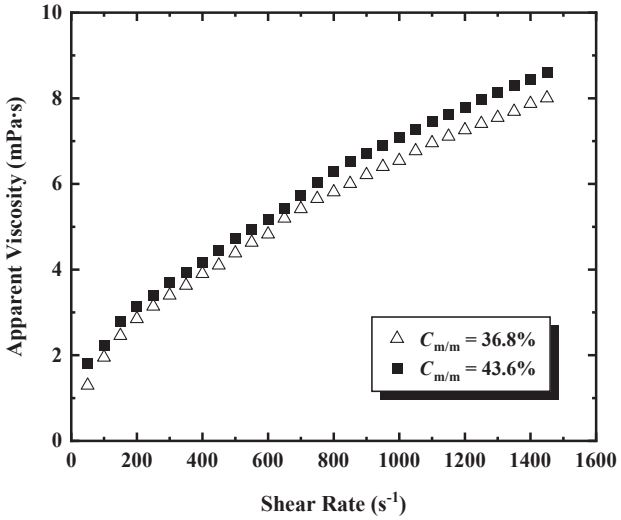

Fig. 3 Apparent viscosity as a function of shear rate, obtained by rotational rheometry.

Table 3 Power Law rheological model for iron ore slurries.

$C_{m/m}$ (%)	Power Law model	R^2
36.8	$\tau = 1.62\times10^{-4}\dot{\gamma}^{1.532}$	0.99
43.6	$\tau = 2.30\times10^{-4}\dot{\gamma}^{1.493}$	0.99

calculated from the rotation values provided by the RheoCompass software. **Fig. 4** presents the Taylor number values as a function of the shear rate for the studied iron ore suspensions. The results depicted in **Fig. 4** show that the values of the Taylor number (*Ta*) for the two suspensions (36.8 % solids versus 43.6 % solids) are very close due to the fact that they were obtained at the same speeds and with the same sensors. Furthermore, the specific gravities of the suspensions were not so distinct: 1363.25 kg/m^3 versus 1483.71 kg/m^3. The results also reveal that the magnitude of *Ta* exhibited values between 41 and 400, except for a shear rate lower than 100 s^{-1}. For this reason, in the experimental conditions investigated, the flow regime was laminar in the presence of Taylor vortices, according to the criterion presented by Shi (2016). Regarding **Fig. 4**, it is observed that the magnitude of *Ta* decreases sharply for shear rates lower than 500 s^{-1}, where particle settling may occur. Therefore, the values of *Ta* obtained in this range may be inaccurate. Therefore, to prove the possible occurrence of flow instabilities and vortices, the conditions defined for the beginning of the vortex formation were applied. These results demonstrate the challenge of characterizing the rheology of mineral slurries consisting of coarse or "dense" particles in rotational devices. High shear rates allow the suspension of particles but favor the occurrence of centrifugal force, secondary flows, Taylor vortices, and turbulence. Conversely, lower shear rates guarantee laminar flows but do not prevent particle sedimentation.

Table 4 Rheological model of Tscheuschner for iron ore slurries.

$C_{m/m}$ (%)	Tscheuschner model	R^2
36.8	$\tau = 0.16+0.27\dot{\gamma} - 0.28\dot{\gamma}^{0.99}$	0.99
43.6	$\tau = 0.20+0.30\dot{\gamma} - 0.31\dot{\gamma}^{0.99}$	0.99

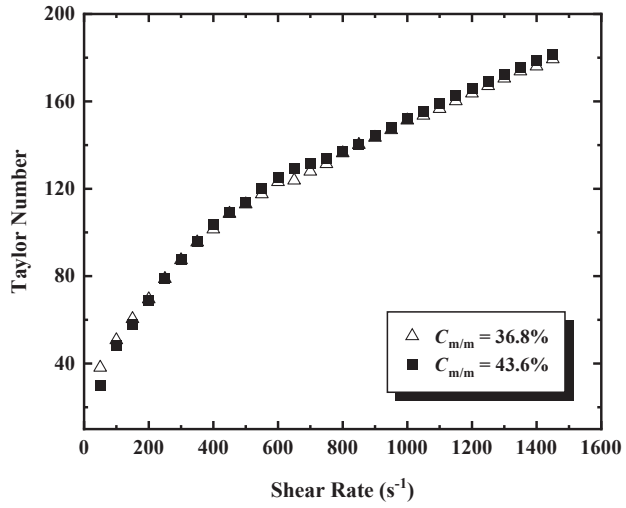

Fig. 4 Taylor number as a function of the shear rate (rotational rheometer).

3.2 Tubular rheometry

3.2.1 Flow curves

The results of the pressure gradient as a function of the mean flow velocity for iron ore slurries are presented in **Fig. 5** and show that the pressure gradient decreases as the mean flow velocity is reduced.

The characteristic behavior of the curves shown in **Fig. 5** indicates that the particles remained suspended throughout the experiment. If there were sedimentation and formation of a bed of particles on the lower parts of the tube (bottom), there would be an increase in the pressure gradient due to the reduction of the sectional area of the tube available for fluid flow.

3.2.2 Friction factor, entropy parameter (*M*) and Reynolds number

Fig. 6 presents the values of the friction factor as a

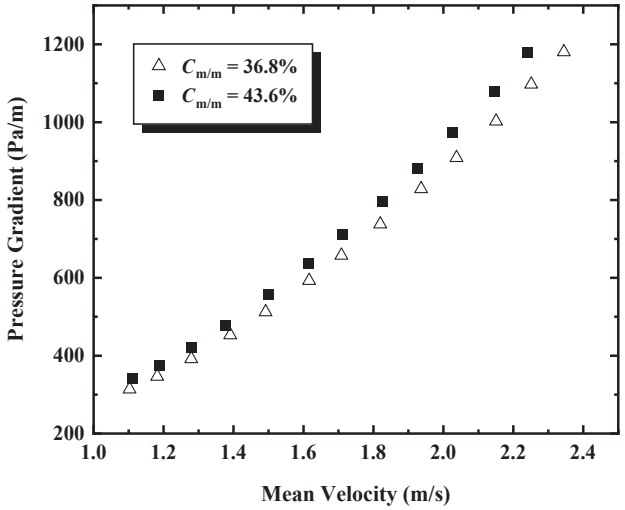

Fig. 5 Pressure gradient as a function of mean flow velocity for iron ore suspensions (tubular rheometer).

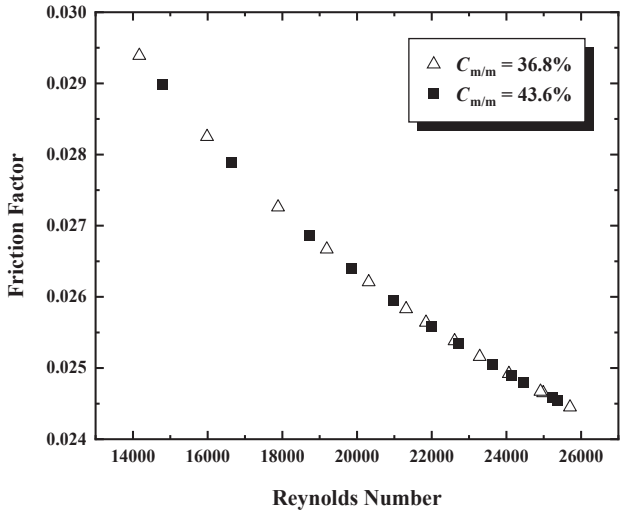

Fig. 6 Friction factor as a function of Reynolds number (tubular rheometer).

function of the Reynolds number for the flow of iron ore suspensions. The results show that the lowest Reynolds numbers for suspensions at 36.8 % and 43.6 % of solids were 14,170.2 and 14,780.9, respectively, indicating turbulent flow.

In addition to being a modeling parameter of the velocity profile, the entropy parameter (M), like the Reynolds number, also indicates the degree of turbulence experienced by a flow. As such, for laminar regime $M = 0$ and for turbulent regime $M > 0$ (Chiu et al., 1993; Souza and Moraes, 2017). Therefore, the friction factor is also presented as a function of the entropy parameter in **Fig. 7**.

The lowest values of M were 3.58 and 3.62, corresponding to slurries with 36.8 % and 43.6 % of solids, respectively, corroborating the state of turbulence indicated by the magnitude of the Reynolds numbers (**Fig. 6**). A realistic rheological characterization of particulate systems requires that the particles be homogeneously suspended in the carrier fluid. Flows with beds of sedimented particles reveal the co-existence of "different fluids" because of the different concentrations of solids along the cross-section of the tube.

3.2.3 Rheograms

The results of shear stress as a function of shear rate for the iron ore slurries are shown in **Fig. 8**. For the slurry at 36.8 % solids (mass basis), the lowest and highest shear rates were 739.86 s^{-1} and 2373.24 s^{-1}, respectively. In relation to the suspension prepared at a solids concentration of 43.6 %, the lowest and highest rates were 766.05 s^{-1} and 2236.68 s^{-1}, respectively. In this way, it is verified that the tubular device allows for much higher shear rates than those obtained from the laboratory Anton Paar rotational rheometer.

The Power Law model was fitted to the rheological curves presented in **Fig. 8**, and the consistency (K) and behavior (n) indices are reported in **Table 5**. The magnitudes of (n) revealed that the iron ore slurries behaved as shear-thinning fluids in the intervals that included the lowest shear rates ($n < 1.0$) and shear-thickening in the intervals that comprised the highest rates ($n > 1.0$), in the two solid concentrations investigated. Shear-thickening behavior is classified as continuous because the viscosity increases smoothly with increasing shear rate and the magnitude of n is between 1 and 2 (Brown and Jaeger, 2014).

Fig. 9 presents the results of the apparent viscosity as a function of shear rate, in which a reduction of the apparent viscosity is verified in the three lowest rates (shear-thinning behavior) and an increase in the others (shear-thickening behavior). For particulate suspensions (slurries), both shear-thinning and shear-thickening behavior observed at low and high shear rates have been reported (Brown and Jaeger, 2014; Stickel and Powell, 2005).

Shear-thinning behavior at lower rates may have been caused by the stratification of particles arranged in layers oriented in the direction of flow (Gürgen et al., 2017). This flow condition was identified in the work of Souza Pinto et al. (2014), who performed pumping experiments with slurries of hematite, quartz, and apatite in devices with internal diameters of 25.4 mm and 50.8 mm. Sampling the flows in three sections of the pipe concluded that, for the three

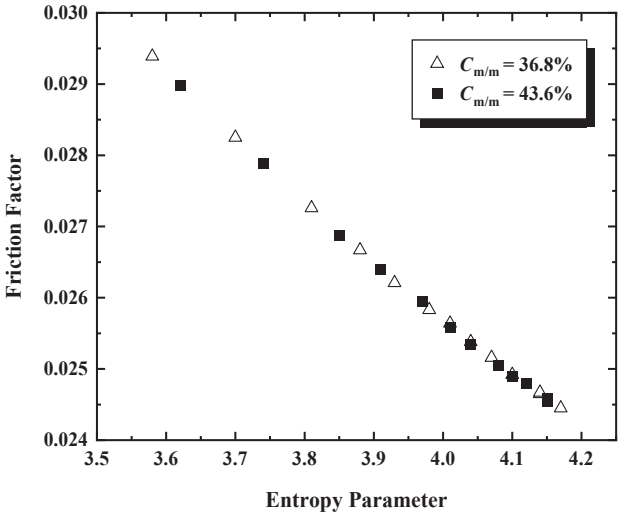

Fig. 7 Friction factor as a function of the entropy parameter.

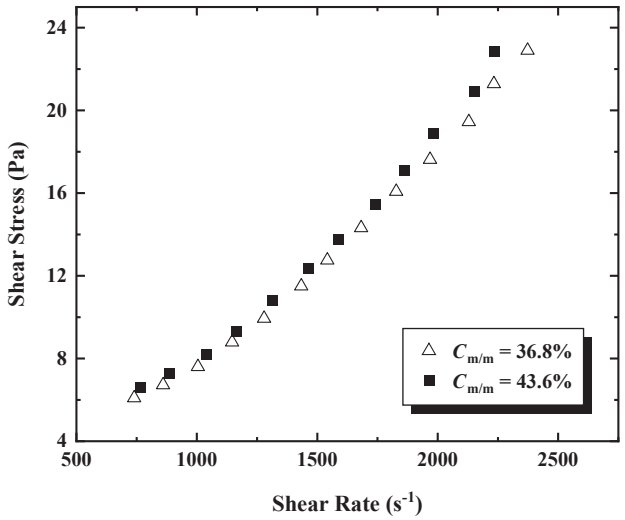

Fig. 8 Shear stress as a function of the shear rate for iron ore slurries.

Table 5 Fitting parameters of the Power Law rheological model ($R^2 = 0.99$) applied to the rheograms obtained from tubular rheometry.

$C_{m/m}$ (%)	Shear rate (s^{-1})	K (Pa·s^n)	n
43.6	766.05–1038.54	0.065	0.69
43.6	1038.54–2236.68	5.76×10^{-4}	1.36
36.8	739.86–1004.65	0.049	0.78
36.8	1004.65–2373.24	7.43×10^{-4}	1.32

minerals studied, more than 60 % of the mass of solids was contained in the lower section of the pipes. On the other hand, the shear-thickening behavior may be due to the formation of particle agglomerates, called hydro clusters, and the hydrodynamic lubrication effects between particles at high shear rates (Salunkhe et al., 2018).

Hydroclusters are particle agglomerates that exhibit greater resistance to flow. Regarding the formation of hydroclusters, Seto et al. (2013) argued that in pipe flow, particles are "pushed" along a "compression axis". This effect is intensified when high shear rates are applied, thus decreasing the distance between particles. The particles agglomerates that may form as they approach will offer greater resistance to flow. In addition to the lubrication effect, friction between the rough surfaces of the particles may occur, which promotes an increase in viscosity (Seto et al., 2013).

In addition to the aforementioned effects, turbulence influences the rheological behavior of suspensions. Fox et al. (2006) defined turbulence as a phenomenon that is almost always undesirable because it creates greater resistance to flow, thus contributing to an increase in the apparent viscosity of the fluid. In this type of flow, random fluctuations in velocity are responsible for Reynolds stresses, which are associated with the high kinetic energy of the flow (Groisman and Steinberg, 2000) and act in the transfer of momentum between adjacent layers of fluid (Fox et al., 2006). Vortices in turbulent flows increase energy dissipation and the local shear rate in the fluid (Brown and Jaeger, 2014). Turbulence can also contribute to shear-thickening behavior because of the disorderly and chaotic movement of fluid elements, which obviously increases the probability of contact and friction between particles. Therefore, in the present study, the shear-thickening behavior of the suspensions may have been caused by the concomitant action of interactions between particles (collision, friction and lubrication) and turbulence.

3.3 Tubular rheometry versus rotational rheometry

The results of rotational and tubular rheometry for the iron ore slurries were presented concomitantly in a single curve, called in this study as "universal rheograms", which comprise a very wide range of shear rates. The rheological curves corresponding to the slurry at 36.8 % solids (**Figs. 10** and **11**) were based on shear rate values between 50.01 s^{-1} and 2,373.24 s^{-1}. For the slurry bearing 43.6 % solids, the shear rate values ranged from 50.01 s^{-1} to 2,236.68 s^{-1}, as shown in **Figs. 12** and **13**.

Satisfactory adjustment of all results by the Power Law model ($R^2 = 0.995$) indicates shear-thickening behavior. In all the results presented in **Figs. 10**, **11**, **12**, and **13**, there is

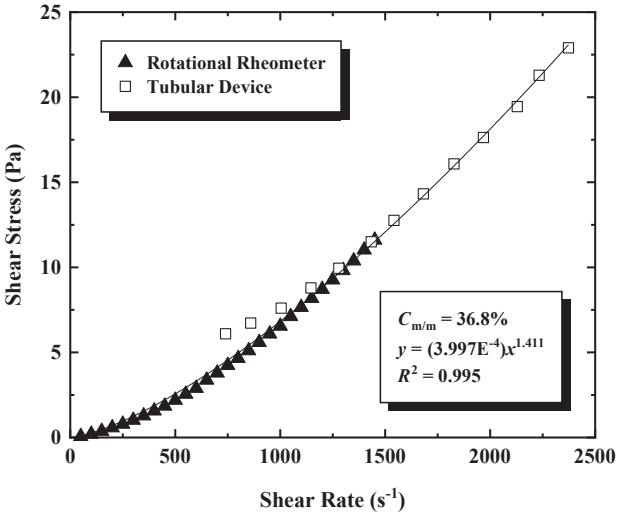

Fig. 10 Shear stress as a function of shear rate obtained by rotational and tubular rheometry for iron ore suspension at 36.8 % solids.

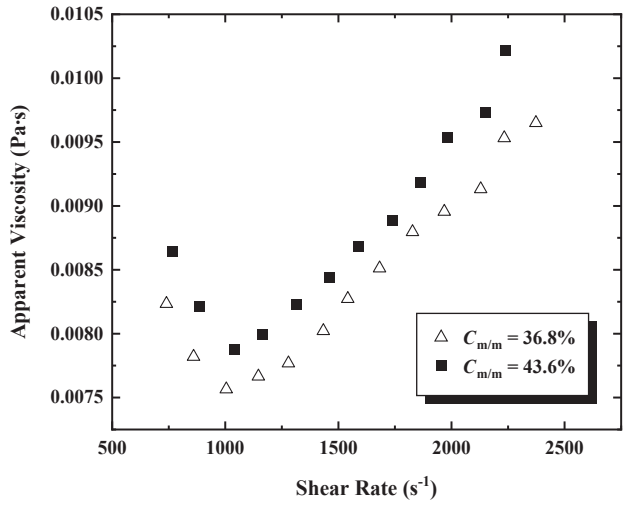

Fig. 9 Apparent viscosity as a function of the shear rate for iron ore slurries.

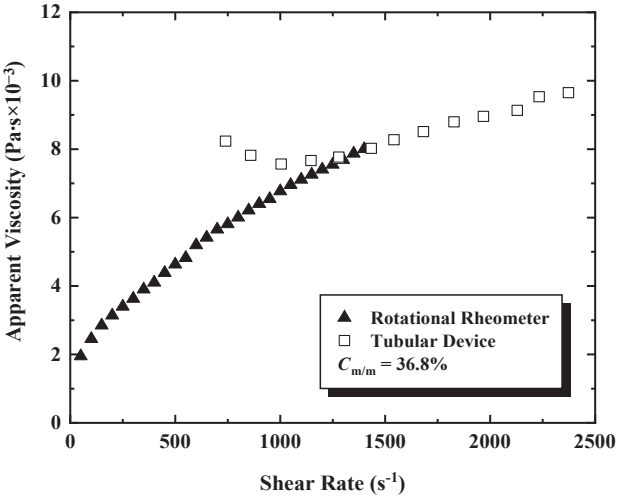

Fig. 11 Apparent viscosity as a function of the shear rate, measured by rotational and tubular rheometry.

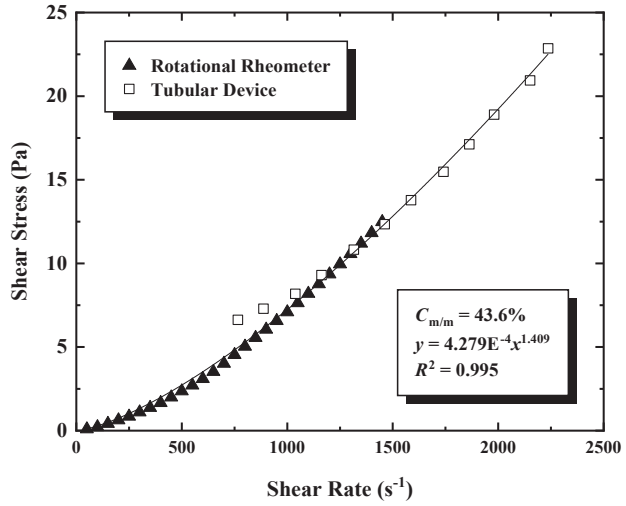

Fig. 12 Shear stress as a function of the shear rate, measured by rotational and tubular rheometry.

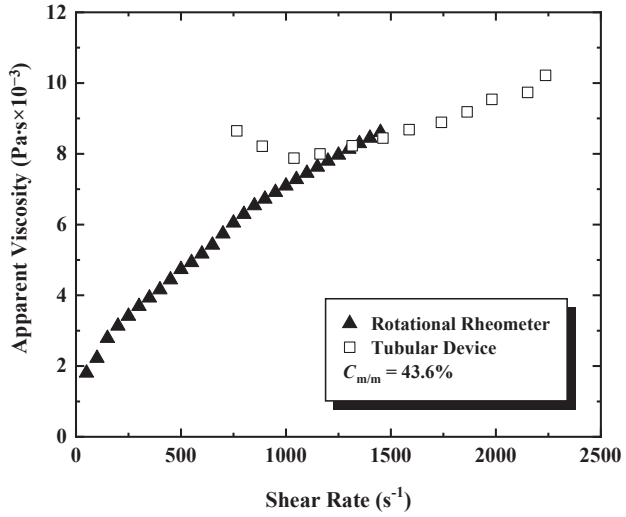

Fig. 13 Apparent viscosity as a function of the shear rate, measured by rotational and tubular rheometry.

a divergence between the rotational and tubular rheometry data within a narrow range of shear rates: from 750 s^{-1} to 1000 s^{-1}.

The characteristics of the flow curves shown in **Fig. 5** do not indicate sedimentation or the formation of a bed of particles in the tube.

However, stratification of particles in the flow may have occurred, which may have caused shear-thinning behavior for values of $\dot{\gamma}_w$ within the narrow range of 750 s^{-1} and 1000 s^{-1}.

4. Conclusions

This work presents and proposes a novel methodology to investigate the rheology of iron ore slurries at two solid concentrations (36.8 % and 43.6 %) via tubular rheometry using the Principle of Maximum Entropy, which provides physically consistent mathematical models that meet the actual features of flow conditions in pipes, such as: typical turbulence levels, high shear rates, and pipe roughness. The results of mean flow velocity and pressure gradient obtained from simple pumping loop tests allowed the calculation of the friction factor, entropy parameter, apparent viscosity of the slurries, and Reynolds number by applying a previously developed model (Louzada et al., 2021). In this way, it was possible to obtain rheograms under shear rates closer to industrial reality ($\dot{\gamma} > 1000$ s^{-1}). In addition, the results obtained from experiments conducted in a laboratory rotational rheometer, under shear rates lower than 1450 s^{-1}, were complemented by those yielded by tubular rheometry at higher shear rates ($\dot{\gamma} \geq 766$ s^{-1}), since both sets of points were satisfactorily adjusted by the Power Law model in a single curve ($R^2 = 0.995$). The rheogram obtained from both complementary techniques was named "universal rheogram" and indicated that the iron ore slurries behaved as shear-thickening fluids ($n > 1$). However, within a narrow range of shear rate (750 $s^{-1} < \dot{\gamma} < 1000$ s^{-1}), three points ($\dot{\gamma}$, τ) obtained from tubular rheometry deviated from the "universal rheogram", showing shear-thinning behavior for the slurry flow. Because the stratification of particles in the pipes may promote fluid shear-thinning behavior, a lack of turbulence in the piping system operating at its lowest shear rates ($\dot{\gamma} < 1000$ s^{-1}) could explain the deviating results. Thus, the range of 750 $s^{-1} < \dot{\gamma} < 1000$ s^{-1} is too high to be applied in laboratory rotational rheometers, due to the occurrence of Taylor vortices, and too low to create enough turbulence to promote adequate particle suspension in pumping loop tubular devices. This is a limitation posed by the novel methodology proposed in this paper.

Acknowledgements

The authors thank CAPES and the Instituto Tecnológico Vale (ITV) for financial support and the Graduate Program in Mineral Engineering at the University of São Paulo.

Nomenclature

PME	Principle of Maximum Entropy
C_L	Correction factor (-)
D	Internal diameter of the tube (m)
f_E	Entropic friction factor (-)
$f(u)$	The probability density function of the velocity
$H(u)$	Entropy of the velocity
K	The consistency of Power Law model (Pa·s^n)
L	Length (m)
M	Entropy parameter, defined as the product of the maximum flow velocity by the second Lagrange multiplier (-)
n'	Correction factor of the Rabinowitsch–Mooney model (-)
ΔP	Pressure drop (Pa)
r	Radial distance (m)
R	Inner radius of the tube (m)
R_e	Radius of the outer cylinder (m)

Re_a	Apparent Reynolds number (-)
R_i	Radius of the inner cylinder (m)
T	Torque (N m)
Ta	Taylor number (-)
u	Velocity (m/s)
$\bar{u}$	Mean flow velocity (m/s)
$u_E(r)$	Entropic velocity distribution (m/s)
u_{ci}	Peripheral velocity of the inner cylinder (m/s)
u_{max}	Maximum flow velocity at the tube center (m/s)
$\dot{\gamma}$	Entropic shear rate (-)
δ	Ratio between the radii of the outer and inner cylinders (-)
η	Apparent viscosity (Pa·s)
ρ	Density (kg m^{-3})
τ	Shear stress (Pa)
τ_0	Yield stress (Pa)
τ_w	Wall shear stress (Pa)
ω	Angular velocity (s^{-1})

Data Availability Statement

Rheology and flow data for iron ore slurries (depicted in **Figs. 2–13**) are available publicly in J-STAGE Data (https://doi.org/10.50931/data.kona.25532392).

References

Barnes H.A., Hutton J.F., Walters K., An Introduction to Rheology, 1st ed., Elsevier, Amsterdam; New York, 1989, ISBN: 9780444871404.

Boger D.V., Rheology and the resource industries, Chemical Engineering Science, 64 (2009) 4525–4536. https://doi.org/10.1016/j.ces.2009.03.007

Brown E., Jaeger H.M., Shear thickening in concentrated suspensions: phenomenology, mechanisms and relations to jamming, Reports on Progress in Physics, 77 (2014) 1–23. https://doi.org/10.1088/0034-4885/77/4/046602

Chhabra R.P., Richardson J.F., Non-Newtonian Flow in the Process Industries, Elsevier, 1999, ISBN: 978-0-7506-3770-1. https://doi.org/10.1016/b978-0-7506-3770-1.x5000-3

Chilton R.A., Stainsby R., Pressure loss equations for laminar and turbulent non-Newtonian pipe flow, Journal of Hydraulic Engineering, 124 (1998) 522–529. https://doi.org/10.1061/(asce)0733-9429(1998)124:5(522)

Chiu C., Entropy and probability concepts in hydraulics, Journal of Hydraulic Engineering, 113 (1987) 583–599. https://doi.org/10.1061/(asce)0733-9429(1987)113:5(583)

Chiu C., Velocity distribution in open channel flow, Journal of Hydraulic Engineering, 115 (1989) 576–594. https://doi.org/10.1061/(asce)0733-9429(1989)115:5(576)

Chiu C., Lin G., Lu J., Application of probability and entropy concepts in pipe-flow study, Journal of Hydraulic Engineering, 119 (1993) 742–756. https://doi.org/10.1061/(asce)0733-9429(1993)119:6(742)

Fangary Y.S., Ghani A.S.A., El Haggar S.M., Williams R.A., The effect of fine particles on slurry transport processes, Minerals Engineering, 10 (1997) 427–439. https://doi.org/10.1016/s0892-6875(97)00019-8

Fox R.W., McDonald A.T., Pritchard P.J., Introdução À Mecânica Dos Fluidos, 6. ed., LTC, Rio de Janeiro (RJ), 2006, ISBN: 9788521614685.

Giguère R., Fradette L., Mignon D., Tanguy P.A., Analysis of slurry flow regimes downstream of a pipe bend, Chemical Engineering Research and Design, 87 (2009) 943–950. https://doi.org/10.1016/j.cherd.2009.01.005

Groisman A., Steinberg V., Elastic turbulence in a polymer solution flow, Nature, 405 (2000) 53–55. https://doi.org/10.1038/35011019

Gürgen S., Kuşhan M.C., Li W., Shear thickening fluids in protective applications: a review, Progress in Polymer Science, 75 (2017) 48–72. https://doi.org/10.1016/j.progpolymsci.2017.07.003

Kawatra S.K., Bakshi A.K., On-line viscometry in particulate processing, Mineral Processing and Extractive Metallurgy Review, 14 (1995) 249–273. https://doi.org/10.1080/08827509508914126

Kawatra S.K., Bakshi A.K., On-line measurement of viscosity and determination of flow types for mineral suspensions, International Journal of Mineral Processing, 47 (1996) 275–283. https://doi.org/10.1016/0301-7516(96)00009-9

Kelessidis V.C., Maglione R., Yield stress of water–bentonite dispersions, Colloids and Surfaces A: Physicochemical and Engineering Aspects, 318 (2008) 217–226. https://doi.org/10.1016/j.colsurfa.2007.12.050

Kitanovski A., Vuarnoz D., Ata-Caesar D., Egolf P.W., Hansen T.M., Doetsch C., The fluid dynamics of ice slurry, International Journal of Refrigeration, 28 (2005) 37–50. https://doi.org/10.1016/j.ijrefrig.2004.07.010

Klein B., Laskowski J.S., Rheological measurements on settling suspensions: characterization of a cyanide leach pulp, Mineral Processing and Extractive Metallurgy Review, 20 (2000) 41–55. https://doi.org/10.1080/08827509908962462

Louzada J.C.G., Souza Pinto T.C., Meier R.G., Souza P.A., Leal Filho L.S., Entropic friction factor modeling for mineral slurry flow in pressurized pipes, Journal of Hydraulic Engineering, 147 (2021) 1–6. https://doi.org/10.1061/(asce)hy.1943-7900.0001934

Lu P., Zhang M., Resistance properties of coal–water paste flowing in pipes, Fuel, 81 (2002) 877–881. https://doi.org/10.1016/s0016-2361(01)00217-4

Ma X., Duan Y., Li H., Wall slip and rheological behavior of petroleum-coke sludge slurries flowing in pipelines, Powder Technology, 230 (2012) 127–133. https://doi.org/10.1016/j.powtec.2012.07.019

Metzner A.B., Reed J.C., Flow of non-Newtonian fluids—correlation of the laminar, transition, and turbulent-flow regions, AIChE Journal, 1 (1955) 434–440. https://doi.org/10.1002/aic.690010409

Mezger T., The Rheology Handbook: For Users of Rotational and Oscillatory Rheometers, 5th revised ed., Vincentz, Hannover, 2020, ISBN: 9783748603702. https://doi.org/10.1515/9783748603702

Mooney M., Explicit formulas for slip and fluidity, Journal of Rheology, 2 (1931) 210–222. https://doi.org/10.1122/1.2116364

Peker S.M., Helvaci S.S., Solid-Liquid Two Phase Flow, 1st ed., Elsevier, Amsterdam; Boston, 2007, ISBN: 9780444522375.

Pereira A.S., Soares E.J., Polymer degradation of dilute solutions in turbulent drag reducing flows in a cylindrical double gap rheometer device, Journal of Non-Newtonian Fluid Mechanics, 179–180 (2012) 9–22. https://doi.org/10.1016/j.jnnfm.2012.05.001

Salunkhe A.A., Overney R.M., Berg J.C., The use of boundary lubricants for the reduction of shear thickening and jamming in abrasive particle slurries, Colloids and Surfaces A: Physicochemical and Engineering Aspects, 537 (2018) 13–19. https://doi.org/10.1016/j.colsurfa.2017.09.029

Senapati P.K., Mishra B.K., Rheological characterization of concentrated jarosite waste suspensions using Couette & tube rheometry techniques, Powder Technology, 263 (2014) 58–65. https://doi.org/10.1016/j.powtec.2014.04.092

Seto R., Mari R., Morris J.F., Denn M.M., Discontinuous shear thickening of frictional hard-sphere suspensions, Physical Review Letters, 111 (2013) 218301-1-218301–218305. https://doi.org/10.1103/PhysRevLett.111.218301

Shi F., Determination of ferrosilicon medium rheology and stability, Minerals Engineering, 98 (2016) 60–70. https://doi.org/10.1016/j.mineng.2016.07.016

Singh V., Sivakumar B., Cui H., Tsallis entropy theory for modeling in water engineering: a review, Entropy, 19 (2017) 1–25. https://doi.org/10.3390/e19120641

Singh V.P., Entropy Theory in Hydraulic Engineering: An Introduction, American Society of Civil Engineers, Reston, Virginia, 2014, ISBN: 9780784412725.

Slatter P., The role of rheology in the pipelining of mineral slurries, Mineral Processing and Extractive Metallurgy Review, 20 (2000) 281–300. https://doi.org/10.1080/08827509908962478

Souza P.A., Moraes E.L., The flow resistance factor treated by the maximum entropy principle, International Journal of Hydraulic Engineering, 6 (2017) 1–8. https://doi.org/10.5923/j.ijhe.20170601.01

Souza Pinto T.C., Moraes Junior D., Slatter P.T., Leal Filho L.S., Modelling the critical velocity for heterogeneous flow of mineral slurries, International Journal of Multiphase Flow, 65 (2014) 31–37. https://doi.org/10.1016/j.ijmultiphaseflow.2014.05.013

Stickel J.J., Powell R.L., Fluid mechanics and rheology of dense suspensions, Annual Review of Fluid Mechanics, 37 (2005) 129–149. https://doi.org/10.1146/annurev.fluid.36.050802.122132

Tozzi E., Hartt W., Non-Newtonian laminar flow in pipes using radius, stress, shear rate or velocity as the independent variable, Physics of Fluids, 33 (2021) 103–104. https://doi.org/10.1063/5.0067993

Whiten W., Steffens P., Hitchins J., An examination of pulp viscosity in tubes at higher shear rates, Minerals Engineering, 6 (1993) 397–404. https://doi.org/10.1016/0892-6875(93)90018-I

Authors' Short Biographies

Prof. Jean Carlo Grijó Louzada is a chemical engineer from the Fluminense Federal University (2006), having obtained a Master of Science degree in metallurgical and materials engineering from the Federal University of Rio de Janeiro (2008) and a Doctor of Science from the Graduate Program Degree in Mineral Engineering (PPGEMin) from the University of São Paulo (2022). He is an associate professor at the Institute of Geosciences and Engineering at the Federal University of South and Southeast Pará.

Elaine Cristina Andrade, MSc, is a materials engineer from the Federal University of Pará (2010), having obtained a master's degree in science from the Technological Institute of Aeronautics (2013). She is currently a doctoral student at the Graduate Program in Mineral Engineering (PPGEMin) at the University of São Paulo.

Dr. Thiago Cesar de Souza Pinto is a chemical engineer from Universidade Santa Cecília (Unisanta), having obtained his master's and doctor's degrees in sciences from the Graduate Program in Mineral Engineering (PPGEMin) at the University of São Paulo. He was a researcher at the Instituto Tecnologico Vale and is currently a researcher at the Mineral Development Center (CDM) of the company Vale S.A.

Prof. Laurindo de Salles Leal Filho obtained a degree in mining engineering from the Federal University of Minas Gerais (1984), a master's degree in metallurgical and mining engineering from the Federal University of Minas Gerais (1988), a doctorate in mineral engineering from the University of São Paulo (1991) and postdoctoral fellow at the Imperial College of Sciences and Technology (1994). Lecturer in the Department of Mining and Petroleum Engineering at the Polytechnic School of the University of São Paulo since 1990, obtaining the associate professorship in 1999 and the position of full professor in 2001. Professor Leal Filho served as scientific director of the Instituto Tecnológico Vale from November 2013 to January 2019.